PAPER

Check for updates

UV-enhanced nano-nickel ferrite-activated peroxymonosulfate for the degradation of chlortetracycline hydrochloride in aqueous solution

Lingxing Zhang, Rui Zhang, Wenna Wang, Shuang Han and Pengfei Xiao (ID) *

In this study, nano-nickel ferrite ($NiFe_2O_4$) was successfully prepared by hydrothermal synthesis and applied to the oxidative removal of chlortetracycline hydrochloride (CTH) in the presence of ultraviolet radiation (UV) and peroxymonosulfate (PMS). Several characterization methods were used to reveal the morphology and surface properties of nano-$NiFe_2O_4$, including X-ray diffraction (XRD), scanning electron microscopy (SEM), and Fourier transform infrared absorption (FTIR) spectroscopy. The removal efficiency of CTH, the factors affecting the reaction process and the reaction mechanism of PMS activated by UV combined with nano-$NiFe_2O_4$ (UV + nano-$NiFe_2O_4$/PMS) in aqueous solution were systematically studied. The results showed that the UV + nano-$NiFe_2O_4$/PMS system led to a higher removal efficiency of CTH than other parallel systems. The results also showed that the CTH removal efficiency was enhanced under optimal conditions ([nano-$NiFe_2O_4$] = 1 g L^{-1}, [PMS] = 1 g L^{-1}, [UV wavelength] = 254 nm and [pH] = 11) and that a removal efficiency of 96.98% could be achieved after 60 min. In addition, the influence of the PMS concentration, CTH concentration, dosage of added nano-$NiFe_2O_4$ and pH on the PMS activation efficiency and CTH oxidative degradation effect was studied. Inorganic anions such as Cl^-, HCO_3^-, CO_3^{2-} and NO_3^- increased the removal efficiency of CTH by 21.29%, 27.17%, 25.32% and 5.96% respectively, while $H_2PO_4^-$ inhibited CTH removal, and the removal efficiency of CTH decreased 6.08% after 60 min. Free radical identification tests detected $SO_4^{-\cdot}$, $OH^\cdot$ and $^1O_2$ and showed that these species participated in the degradation reaction of CTH. The results of LC-MS and TOC analysis showed that CTH was degraded in the UV + nano-$NiFe_2O_4$/PMS system through hydroxylation, demethylation, deamination, and dehydration reaction and finally mineralized into CO_2. These findings confirmed that nano-$NiFe_2O_4$ is a green and efficient heterogeneous catalyst for activation of PMS and demonstrates potential applicability in the treatment of antibiotic wastewater.

1. Introduction

Antibiotics are commonly used anti-infective drugs and have been widely used in human disease prevention and animal husbandry. Although they have made great contributions to the development of health care, antibiotics also threaten the environment.[1–4] Chlortetracycline hydrochloride (CTH) is a tetracyclic broad-spectrum antibiotic, and due to its low price and potential for promoting the growth of livestock, it has been widely used in animal husbandry.[5–7] Nevertheless, the absorption capacity of CTH by humans and animals is limited. These high concentrations of CTH have adverse effects on the ecosystem and human health. This compound is responsible for the inhibition of microbial activity and

growth,[8] phytoplankton toxicity,[9] inhibition of protein synthesis,[10] and endangering the life activities of aquatic organisms. Therefore, CTH is considered an important pharmaceutical pollutant, and its removal from water has become an urgent issue.

Various physical, chemical and biological methods such as electrodynamic technology,[11] photocatalytic technology,[12] microbial treatment[13] and so on have been reported for the removal of CTH from water. Although these methods exhibit a certain removal effect, there are still problems such as high energy consumption and low degradation efficiency. In recent years, advanced oxidation processes (AOPs) have received widespread attention. The oxidation process has proven to be an effective method to degrade stubborn emerging pollutants,[14,15] such as aromatic amine[16] and aromatic alcohols.[17] Almost all traditional oxidation processes involve the generation of hydroxyl radicals ($OH^\cdot$), which are nonselective for

College of Forestry, Northeast Forestry University, Harbin 150040, China. E-mail: xpfawd@nefu.edu.cn

most organic pollutants.[18] Advanced persulfate oxidation technology produces sulfate radicals ($SO_4^-\cdot$), which can overcome the limitations of $OH\cdot$. As an advanced oxidation method, at room temperature, persulfate ions ($S_2O_8^{2-}$) have the advantages of strong stability, solubility, and high oxidation potential ($E_0 = 2.01$ V).[19] Recently, $SO_4^-\cdot$ radical-based processes have attracted significant attention among researchers. $S_2O_8^{2-}$ can be further activated by external energy activators (such as ultrasound, heat and ultraviolet radiation), transition metals (such as iron, cobalt and manganese) and chemical activators (such as alkali, phenol and quinone)[20] to produce $SO_4^-\cdot$.

Iron is a transition metal element and is less toxic than copper, manganese and other metal elements. Iron-based metal activation has been the most studied and reported method for efficient $SO_4^-\cdot$ production.[21,22] In recent years, iron ions have been loaded into ceramics, molecular sieves and other carriers and then applied to advanced oxidation technology.[23] Nickel ferrite ($NiFe_2O_4$) is a promising catalyst for advanced oxidation in practical applications because it is easily immobilized, separated, recovered and reused through application of an external magnetic field.[24]

In this research, we used a hydrothermal synthesis method to prepare nano-$NiFe_2O_4$ as a solid catalyst for the activation of peroxymonosulfate (PMS) and coactivated it with ultraviolet (UV) radiation to explore the oxidative removal of CTH. The nanomaterials were characterized by X-ray diffraction (XRD), scanning electron microscopy (SEM) and Fourier transform infrared (FTIR) spectroscopy. Then we first investigated the removal efficiency of CTH by different systems and the reaction mechanism of PMS activated by UV irradiation combined with nano-$NiFe_2O_4$ (UV + nano-$NiFe_2O_4$/PMS) in aqueous solution. Additionally, the effects of the initial solution pH, catalyst dosage, CTH concentration, PMS concentration and coexisting inorganic ions on the degradation efficiency were discussed. The identification and formation mechanism of oxygen species participated in the degradation reaction of CTH were analyzed in this study. Through LC-MS data analysis, the CTH degradation products were determined. The roles of the catalyst, related oxidative radicals and application potential in the UV + nano-$NiFe_2O_4$/PMS system were also discussed in detail. This study provides a feasible approach to remove CTH for catalytic oxidation in environmental remediation.

2. Experimental

2.1 Chemicals and materials

Standard samples of CTH (98%), potassium monopersulfate ($KHSO_5 \cdot 0.5KHSO_4 \cdot 0.5K_2SO_4$, ≥42% $KHSO_5$ basis), nickel chloride hexahydrate ($NiCl_2 \cdot 6H_2O$, 99%), ferric chloride hexahydrate ($FeCl_3 \cdot 6H_2O$, 97%), sodium hydrosulfide hydrate (Na_2HS, 99%), sodium hydroxide (NaOH, 96%), potassium chloride (KCl, 96%), sodium bicarbonate ($NaHCO_3$, 99.5%), sodium carbonate (Na_2CO_3, 99.8%), *tert*-butanol (TBA, GR, ≥99.5%), methanol (MeOH, AR, ≥99.5%), ethanol (EtOH, AR, ≥99.5%), and furfuryl alcohol (FFA, CP, ≥97%) were purchased from Aladdin Industrial Corporation (Shanghai, China).

Ultrapure water was used in the experiments, and all chemical reagents in the experiments were analytically pure.

2.2 Synthesis of reduced nano-$NiFe_2O_4$

Nano-$NiFe_2O_4$ was synthesized by a hydrothermal synthesis method. First, 3.5652 g of $NiCl_2 \cdot 6H_2O$, 8.1002 g of $FeCl_3 \cdot 6H_2O$ and 5.12 g of NaOH were dissolved in 250 mL of deionized water. Then, the dissolved $NiCl_2$ solution and dissolved $FeCl_3$ solution were mixed thoroughly, 8.65 g of Na_2HS was added, and the solution was stirred until the mixture became a creamy yellow (JB-3 timing thermostatic magnetic mixer, Leicixinjing Shanghai, China). The pH of the mixed solution was adjusted to 11 with NaOH while the solution was stirred continuously and refluxed at 120 °C (DHG-9023AD, Qixin Shanghai, China) for 2 h. After the product temperature decreased to room temperature, it was cleaned with deionized water three times and then cleaned with absolute ethanol three times. Next, the product was dried at 100 °C. Finally, the black powder was calcined at 600 °C for 4 h and grinded the sample until could pass through a 2 nm sieve, the sample was labelled "nano-$NiFe_2O_4$". The entire reaction was completed in about 2 hours time.

2.3 Experimental procedures

Degradation experiments of CTH were carried out to evaluate the catalytic performance of the doped nano-$NiFe_2O_4$ catalysts. All of the experiments were carried out at room temperature and performed under a UV lamp (254 nm, ZF-8, YuMing Shanghai, China). The UV lamp was turned on 20 min before the beginning of the experiments to obtain a stable level of UV irradiation. The initial concentration of CTH was 120 mg L^{-1}, and 50 mL of this solution was added to the reaction flask. Then, the initial concentrations of PMS (1 g L^{-1}) and the initial of nano-$NiFe_2O_4$ (1 g L^{-1}) were added to the experimental system at the initial pH = 2.7. The pH of the experimental system was adjusted by using 1 M NaOH, 0.1 M NaOH and 0.1 M HCl. The samples were collected at set time points (10, 20, 30, 40, 50, and 60 min) with a plastic syringe and filtered through a 0.45 μm filter. Then, the absorbance of CTH in the solution was measured at 364 nm using a UV-vis spectrophotometer. Finally, the concentration of CTH was calculated from the standard curve, and then, the removal efficiency of CTH was calculated.

2.4 Analytical methods

A UV-vis spectrophotometer (UV-1800, HACH, USA) was employed to measure the concentrations of CTH using a spectrophotometric method at the characteristic wavelength of 364 nm. The pH values were determined by using an FE20 precision pH meter (Mettler Toledo, Zurich, Switzerland). TOC measurements were carried out with a TOC-LCPN analyzer (TD-3500, Dandong, China).

A UV-vis spectrophotometer (TU-1901, Beijing General Analysis, China) was used to scan from 190 to 500 nm to obtain the ultraviolet-visible (UV-vis) absorption spectrum. The surface morphology and microstructure of synthetic materials were observed by scanning electron microscopy (SEM) (su8020, Hitachi, Japan). X-ray diffraction (XRD) (TD-3500, Dandong,

China) was used to determine the crystal structure of the material. The surface functional groups of the material were measured by Fourier transform infrared (FTIR) spectrometer (iS10 FT-IR spectrometer, Nicolet, USA). The free radicals produced during the process were determined using electron paramagnetic resonance (EPR) spectroscopy (A300-10/12, Bruker, Germany). A liquid chromatography-mass spectrometry (LC-MS) system (chromatography: U3000, Thermo Fisher Scientific, USA; mass spectrometry: Q Exactive, Thermo-FID, USA) was used to detect intermediate substances produced during the reaction.

3. Results and discussion

3.1 Characterization of nano-$NiFe_2O_4$

The morphology of nano-$NiFe_2O_4$ was observed by field emission SEM.[25] The crystalline structure of nano-$NiFe_2O_4$ was investigated by XRD.[26] FTIR[27] spectroscopy was used to detect the forms of the main elements in the sample.

The morphology of nano-$NiFe_2O_4$ was observed by SEM. As shown in Fig. 1a and b, the material had a loose nano-microstructure with a primary particle size of 20–50 nm and a secondary particle size of 5–10 μm. The particle sizes reveal the agglomeration of particles, which can be ascribed to the heat released from combustion. Due to the heat generated during the combustion reaction, not only agglomeration but also the sintering of small particles is observed.[28] After the agglomeration of nanoparticles, micron-scale particles were formed. The particle structure was relatively loose, and there were many gaps, as shown in the red circle in Fig. 1a. Loose nanostructural particles had a higher specific surface area and

could therefore come into contact with more reactants; hence, the catalytic effect was better than that of other catalysts. Fig. 1c and d shows SEM images of the nano-$NiFe_2O_4$ recovered after the reaction. It can be seen from the figure that the pores of nano-$NiFe_2O_4$ decreased after the reaction and that the reactant was adsorbed and then reacted on the catalyst surface. It could be proved that the nano-$NiFe_2O_4$ has a adsorption effect.

The XRD patterns of nano-$NiFe_2O_4$ before and after the reaction are shown in Fig. 2a. By comparing the XRD patterns of nano-$NiFe_2O_4$, it can be seen that the nanoparticles did not undergo a phase change after the catalysis treatment.[29] The corresponding card is PDF# 00-54-0964. According to the card, the corresponding phase was a cubic phase, the space group was $Fd\bar{3}m$ (227), and the lattice parameters of the corresponding PDF card were $A = B = C = 8.3393$ and $\alpha = \beta = \gamma = 90°$. The diffraction peaks of nano-$NiFe_2O_4$ show that the structure of $NiFe_2O_4$ is a hexagonal crystal structure with a miller index specific at (220), (311), (222), (400), (422), (511), (440) and (533). There is almost no impurities in Fig. 2a, which proves that the sample is relatively pure. As shown in Fig. 2a, the measured XRD was offset to the right, indicating that the lattice parameters of the material were relatively small. By comparing the peak positions before and after treatment, it could be seen that the lattice constant of the material did not change after adsorption, which indicated that the stability of nano-$NiFe_2O_4$ was high. Moreover, the peak strength showed that the peak after adsorption was relatively high and sharp, which might be caused by grain agglomeration. Grain agglomeration might lead to a decrease in the adsorption capacity of the material.

As shown in Fig. 2b, there were obvious infrared stretching vibration peaks at approximately 602, 1630 and 3435 cm^{-1}, of
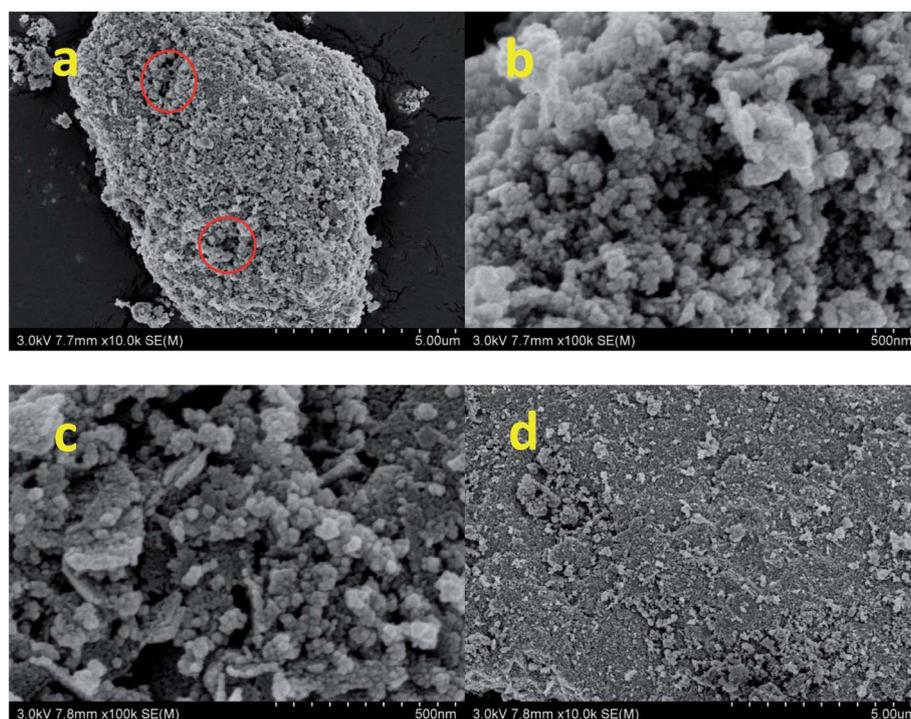

Fig. 1 SEM image of nano-$NiFe_2O_4$ before the reaction (a and b) and the nano-$NiFe_2O_4$ after the reaction (c and d).
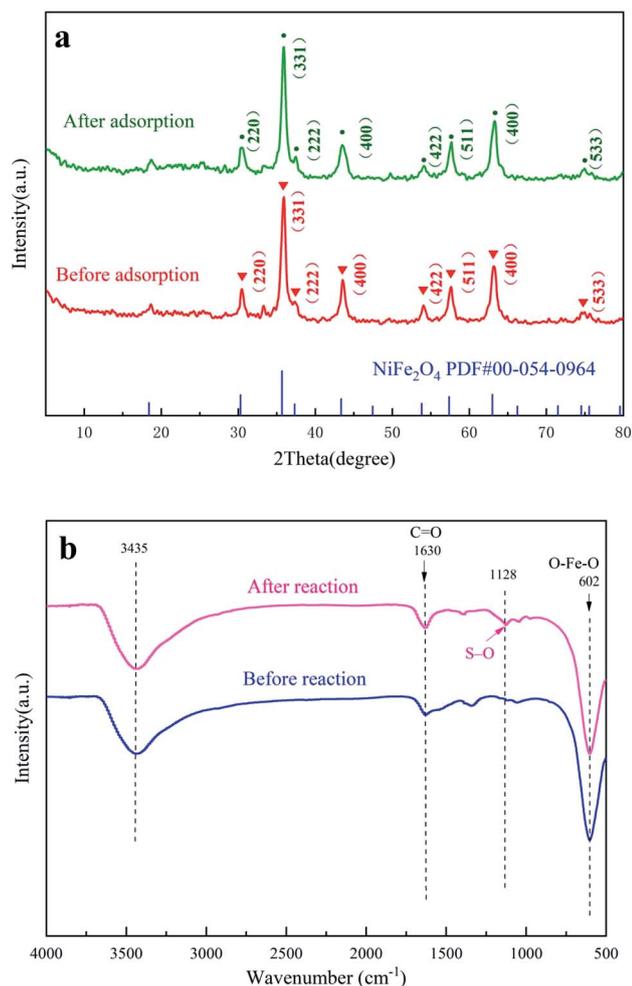
Fig. 2 XRD patterns of nano-NiFe$_2$O$_4$ (a), FT-IR diagram of nano-NiFe$_2$O$_4$ (b).

which 602 cm^{-1} was the stretching vibration of O–Fe–O, 3435 cm^{-1} was the stretching vibration peak of hydroxyl-adsorbed water on the surface, and 1630 cm^{-1} was the C=O vibration peak. The stretching vibration of O–Fe–O did not change significantly after the reaction, which indicated that the structure of nano-NiFe$_2$O$_4$ was not destroyed after advanced oxidation. In addition, the nano-NiFe$_2$O$_4$ had an infrared peak at 1128 cm^{-1} that appeared only after the reaction, which belonged to an S–O vibration. This signal might have been caused by the adsorption of SO$_4^{2-}$ generated after the activation of persulfate on the surface of nano-NiFe$_2$O$_4$.

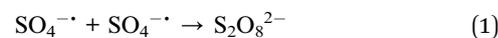### 3.2 Removal efficiency of CTH in different systems

To investigate the removal efficiency of CTH by different systems, experiments were conducted under the following conditions: the dosage of nano-NiFe$_2$O$_4$ was 1 g L^{-1}, the initial concentration of PMS was 1 g L^{-1}, the initial concentration of CTH was 60 mg L^{-1}, pH = 2.7 and the reaction time was 60 min. Fig. 3 depicts the removal efficiency of CTH under different reaction conditions.

This result shows that UV irradiation alone was the least efficient method of removing CTH. This result indicated that

CTH did not easily photodegrade in the absence of catalyst, which could be explained by its UV photostability. The removal efficiency of CTH was over 30% after 10 min in both the nano-NiFe$_2$O$_4$ system and UV/nano-NiFe$_2$O$_4$ system; however, after that point, there was no significant change in the removal of CTH in the reaction, which could be explained by the removal of CTH being mainly due to the adsorption of CTH by nano-NiFe$_2$O$_4$.[30] When only PMS was present in the system, the removal efficiency reached 43.98% after 60 min. Previous studies have found that CTH cannot be oxidized efficiently with PS used alone.[31] By the addition of UV irradiation to activate PMS, the CTH concentration decreased, and the removal efficiency reached 47.07%, still at a low level, which indicated that the efficiency of PMS generated by UV activation alone was limited. In contrast, when nano-NiFe$_2$O$_4$ was added to the PMS system, the removal efficiency reached 69.31%. It was found that the new system could effectively activate PMS and produce SO$_4^{-\cdot}$, thus rapidly oxidizing and removing CTH. In the UV + nano-NiFe$_2$O$_4$/PMS system, the removal efficiency reached 72.07% after 60 min, which was higher than the removal efficiencies of PMS, nano-NiFe$_2$O$_4$/PMS, UV/PMS and other systems. This result indicated that nano-NiFe$_2$O$_4$ combined with UV irradiation has a good coordination effect; consequently, the efficiency of the combination to activate PMS to produce SO$_4^{-\cdot}$ could be improved.

3.3 Influences of several parameters on CTH removal in the UV + nano-NiFe$_2$O$_4$/PMS system

3.3.1 PMS concentration. The removal efficiency of CTH affected by different PMS concentrations (0.2, 0.4, 1.0 and 2.0 g L^{-1}) under initial conditions (dosage of nano-NiFe$_2$O$_4$ was 1 g L^{-1}, concentration of CTH was 60 mg L^{-1}) is illustrated in Fig. 4a. With increasing PMS concentration from 0.2 g L^{-1} to 1 g L^{-1}, the removal efficiency of CTH gradually increased from 63.35% to 70.73%. The degradation rate was faster at higher initial PMS concentration. It can be explained that the production of free radicals (SO$_4^{-\cdot}$, HO$^{\cdot}$) was in proportion to PMS concentration at a certain temperature. More active radicals (SO$_4^{-\cdot}$, HO$^{\cdot}$) were produced at high PMS concentrations to removal CTH. However, Fig. 4a shows that there was little difference in the CTH removal efficiency when the PMS concentration was 1 g L^{-1} and 2 g L^{-1}. Thus, increasing the concentration of PMS did not simultaneously increase the speed of removal indefinitely. The reason was that increased concentrations of PMS generated more reactive oxygen species as well as SO$_4^{-\cdot}$, but PMS could react with SO$_4^{-\cdot}$ to form radicals with weaker oxidative capacity and lead to self-quenching,[32] as shown in eqn (1) and (2). As the PMS concentration increased, the scavenging rate of SO$_4^{-\cdot}$ might have been faster than the production rate, leading to a decrease in the concentration of SO$_4^{-\cdot}$, and therefore, the removal of CTH could have become inhibited.[33,34]

$$SO_4^{-\cdot} + SO_4^{-\cdot} \rightarrow S_2O_8^{2-} \qquad (1)$$

$$SO_4^{-\cdot} + S_2O_8^{2-} \rightarrow SO_4^{2-} + S_2O_8^{-\cdot} \qquad (2)$$
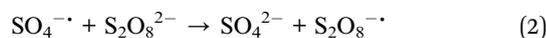
3.3.2 CTH initial concentration. The effect of the CTH concentration on removal was studied, and the results are presented in Fig. 4b. The experiment was conducted under the following conditions: the dosage of nano-NiFe$_2$O$_4$ was 1 g L^{-1} and the concentration of PMS was 1 g L^{-1}.

When the initial concentration was increased from 20 to 100 mg L^{-1}, the removal efficiency of CTH decreased from 99.7% to 66.87%. With the initial conditions unchanged, the removal efficiency of CTH was negatively correlated to its initial concentration. Increasing the concentration of CTH might promote the effective collision between CTH and radicals (SO$_4^{-\cdot}$, HO$^{\cdot}$); nevertheless, the total radical (SO$_4^{-\cdot}$, HO$^{\cdot}$) yields were constant once the dosage of PMS became constant under the corresponding conditions. As a consequence, when the initial CTH concentration was increased, the removal efficiency of CTH decreased during the reaction time.

3.3.3 Nano-NiFe$_2$O$_4$ dosage. The removal efficiency of CTH in the UV + nano-NiFe$_2$O$_4$/PMS system with different nano-NiFe$_2$O$_4$ dosages was studied when the concentration of PMS was 1 g L^{-1} and the initial concentration of CTH was 60 mg L^{-1}. The results are presented in Fig. 4c. The influence of the nano-NiFe$_2$O$_4$ dosage on CTH removal was not obvious in the first 10 min. Then, increasing the nano-NiFe$_2$O$_4$ dosage from 0.5 to 2 g L^{-1} led to a faster and more efficient removal of CTH with the efficiency increasing from 68.53% to 79.65%. These results could be explained by the high concentration of SO$_4^{-\cdot}$ formed under the condition of a higher nano-NiFe$_2$O$_4$ dosage, thereby leading to an increase in the removal efficiency of CTH. Secondly, the observed increase could be attributed to the presence of a large surface area of the adsorbent when the dosage was increased which provided more active binding sites.[35] Nevertheless, as the nano-NiFe$_2$O$_4$ dosage was further increased to 2 g L^{-1}, the removal efficiency decreased. An excessive concentration of SO$_4^{-\cdot}$ formed, enabling these radical ions to react with each other, causing a decrease in the SO$_4^{-\cdot}$ concentration that led to a decreased removal efficiency of CTH. Excessive Fe^{2+} release from nano-NiFe$_2$O$_4$ at a relatively high dosage would also consume a large amount of SO$_4^{-\cdot}$,[36–38] as shown in eqn (3). In addition, high levels of nano-NiFe$_2$O$_4$ in solution resulted in an increase in self-aggregation, thus reducing the total number of active sites.

$$Fe^{2+} + SO_4^{-\cdot} \rightarrow SO_4^{2-} + Fe^{3+} \tag{3}$$
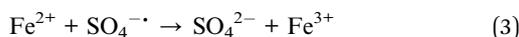
3.3.4 Initial solution pH. The process of removing CTH in the UV + nano-NiFe$_2$O$_4$/PMS system was directly influenced by the pH value. In this research, the influence of initial pH was investigated under the following conditions: the initial pH was set to 3.0, 5.0 and 11.0; the dosage of nano-NiFe$_2$O$_4$ was 1.0 g L^{-1}; and the initial CTH concentration was 60 mg L^{-1} at room temperature. Fig. 4d shows that the removal efficiency of CTH improved with increasing pH. The maximum CTH removal efficiency at pH = 11 was 98%. Previous studies have shown that SO$_4^{-\cdot}$ yields remain constant under different pH conditions[39,40] and oxidation of 1,1,1-trichloroethane by thermally activation persulfate demonstrated that the reaction rate decreased with

increasing pH.[41] It suggest that the different performances in pH effects could be ascribed to the molecule structure of contaminants and mechanisms of degradation; however, SO$_4^{-\cdot}$ can react with water and OH$^-$ to form OH$^{\cdot}$.[42] Since the rate constant of the reaction between SO$_4^{-\cdot}$ and OH$^-$ is 5 orders of magnitude greater than that between SO$_4^{-\cdot}$ and water, alkaline conditions could promote the generation of OH$^{\cdot}$ in the system.[33] Nevertheless, inhibition experiments[43] have shown that SO$_4^{-\cdot}$ and OH$^{\cdot}$ play a major role under weakly basic conditions (pH < 9), but OH$^{\cdot}$ and ^{1}O$_2$ are the main active species under strongly basic conditions (pH > 9).[44,45] PMS was activated by the base to produce ^{1}O$_2$, which removed CTH [eqn (4)–(14)].[46] In addition, the reactivity of ^{1}O$_2$ could be enhanced due to the smaller size of nano-NiFe$_2$O$_4$;[47] these trends explain why the removal efficiency of CTH is increased under alkaline conditions.
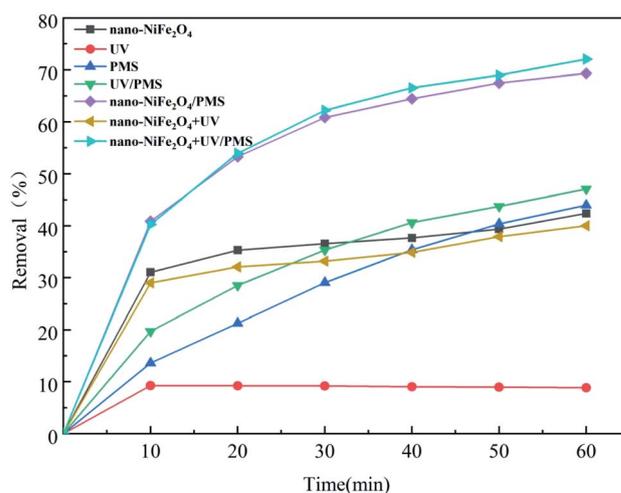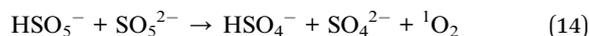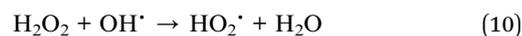
$$HSO_5^- \rightarrow H^+ + SO_5^{2-} \tag{4}$$

$$HSO_5^- + H_2O \rightarrow HSO_4^- + H_2O_2 \tag{5}$$

$$SO_5^{2-} + H_2O \rightarrow SO_4^{2-} + H_2O_2 \tag{6}$$

$$H_2O_2 \rightarrow H^+ + HO_2^- \tag{7}$$

$$HSO_5^- + HO_2^- \rightarrow H_2O + SO_4^{-\cdot} + O_2^{-\cdot} \tag{8}$$

$$H_2O_2 \rightarrow 2OH^{\cdot} \tag{9}$$

$$H_2O_2 + OH^{\cdot} \rightarrow HO_2^{\cdot} + H_2O \tag{10}$$

$$HO_2^{\cdot} \rightarrow H^+ + O_2^{-\cdot} \tag{11}$$

$$OH^{\cdot} + O_2^{-\cdot} \rightarrow {}^1O_2 + OH^- \tag{12}$$

$$2O_2^{-\cdot} + 2H^+ \rightarrow {}^1O_2 + H_2O_2 \tag{13}$$
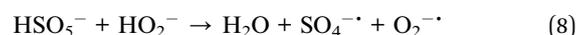
$$HSO_5^- + SO_5^{2-} \rightarrow HSO_4^- + SO_4^{2-} + {}^1O_2 \tag{14}$$
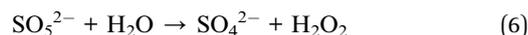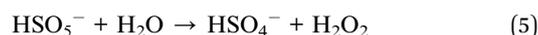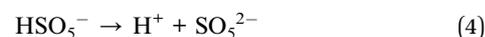

Fig. 3 Effects of different systems on the removal of CTH; the above experimental basic condition: [nano-NiFe$_2$O$_4$] = 1 g L^{-1}, [CTH] = 60 mg L^{-1}, [PMS] = 1 g L^{-1}, [UV wavelength] = 254 nm, pH = 2.7.

3.3.5 Co-existing inorganic ions. Cl^-, HCO_3^-, CO_3^{2-}, NO_3^-, and $H_2PO_4^-$ are widely present in various natural waters and wastewaters. These five ions were added to the system at a concentration of 50 mM and their effects on CTH removal in the UV + nano-$NiFe_2O_4$/PMS system under other fixed experimental conditions are shown in Fig. 4e. Three anions, Cl^-, HCO_3^- and CO_3^{2-}, noticeably increased the removal efficiency of CTH. Compared with the system without any anion addition, the UV + nano-$NiFe_2O_4$/PMS system with Cl^-, HCO_3^-, and CO_3^{2-} added at the end of the reaction increased the removal efficiency by 21.29%, 27.17% and 25.32%, respectively. However, the removal process of CTH differed in the presence of those three different ions. The promotion of the CTH removal efficiency by HCO_3^- and CO_3^{2-} was immediately apparent at the beginning 10 min of the reaction, while the influence of Cl^- was gradually revealed as the reaction proceeded and was not initially obvious. It is well known that the $OH^\bullet$ or H^+ species can be consumed by CO_3^{2-} or HCO_3^- to produce $CO_3^{-\bullet}$, which is much more selective than $OH^\bullet$ for the degradation of organic species such as phenols, anilines, or amino acids [eqn (15)–(17)]. In this context, $SO_4^{-\bullet}$, $CO_3^{-\bullet}$, $^1O_2$ work together to improved removal efficiency of CTH.[48] On the other hand, HCO_3^- and CO_3^{2-} underwent hydrolysis in water, increasing the pH of the solution; hence, this process could promote the activation of PMS and improve the removal efficiency of CTH.[49]
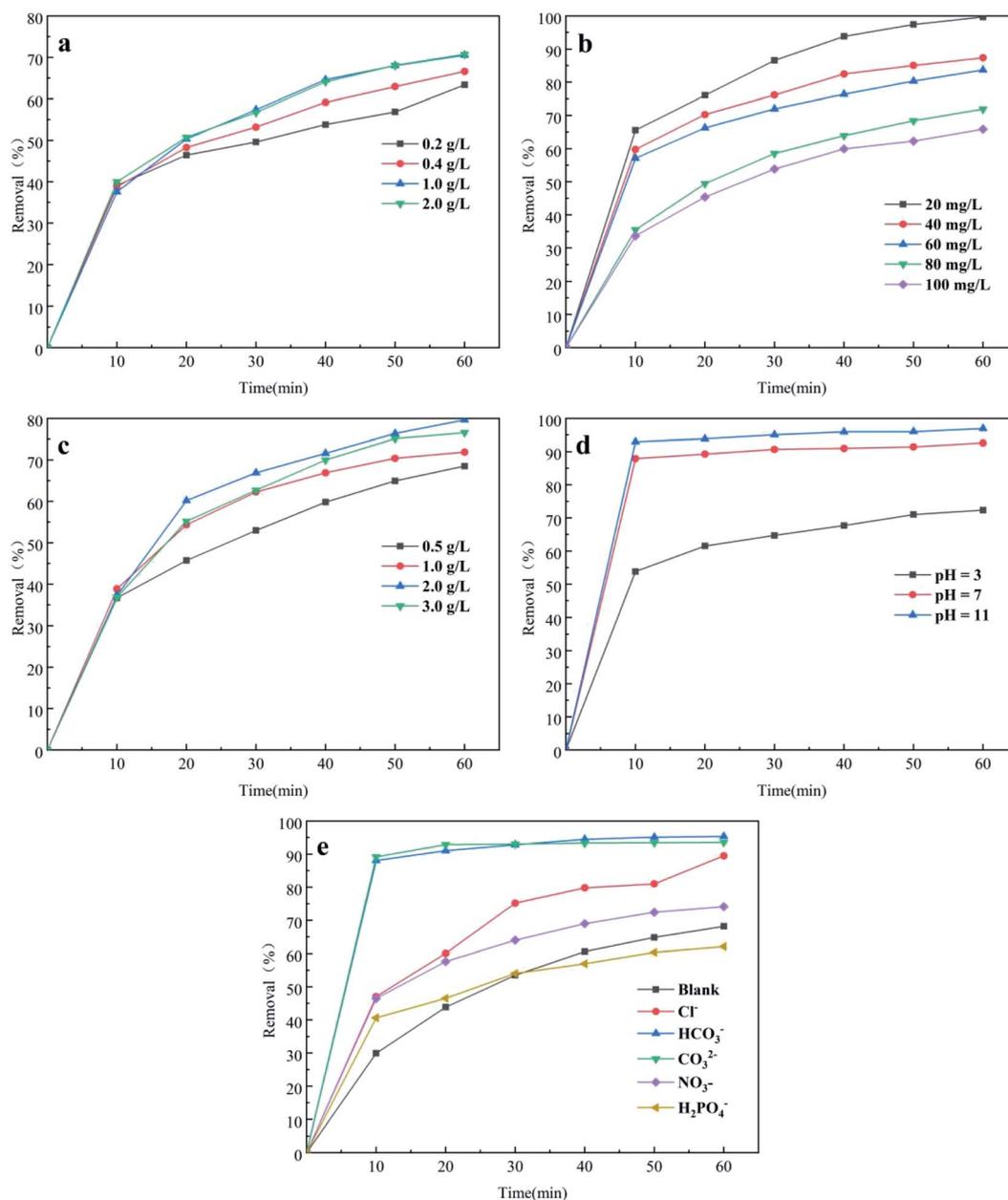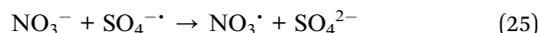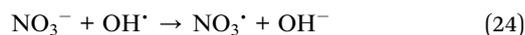

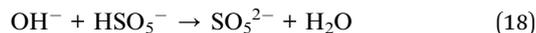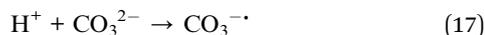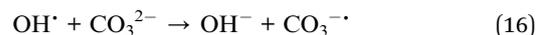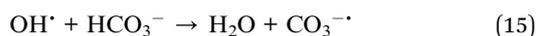Fig. 4 Effect of PMS concentrations (a), initial CTH concentration(b), nano-$NiFe_2O_4$ dosage (c), initial solution pH (d), co-existing inorganic ions (e) on UV/nano-$NiFe_2O_4$ activated PMS system for the removal of CTH; the above experimental basic condition: pH = 2.7.

In addition, PMS could oxidize HCO_3^- to produce a two-electron oxide HCO_4^- [eqn (18) and (19)], which could promote CTH removal.[50,51] Cl^- reacted with HSO_5^- to produce strongly oxidizing HClO, which was further ionized to obtain ClO^-, thereby enhancing the removal of CTH [eqn (20)–(23)].[52,53] Fig. 4e shows that the removal efficiency of CTH increased slightly with the addition of NO_3^- Previous studies have shown that NO_3^- can react with $OH^{\bullet}$ and $SO_4^{-\bullet}$ to generate $NO_3^{\bullet}$ [eqn (24) and (25)]. The propagation reaction of $NO_3^{\bullet}$ generates secondary radicals such as $NO^{\bullet}$, which then reacts with contaminants.[54,55] The addition of phosphate species ($H_2PO_4^-$) inhibited CTH removal. Compared with the system without any addition, the removal efficiency of CTH decreased by 6.08% after 60 min. Iron ions can rapidly form different complexes with $H_2PO_4^-$ and decrease the available soluble Fe^{2+} for PMS activation.[56] In addition, $H_2PO_4^-$ is ionized in water to produce H^+, leading to a decrease in pH. According to previous experiments, the removal efficiency of CTH was low under acidic conditions.

$$OH^{\bullet} + HCO_3^- \rightarrow H_2O + CO_3^{-\bullet} \tag{15}$$

$$OH^{\bullet} + CO_3^{2-} \rightarrow OH^- + CO_3^{-\bullet} \tag{16}$$

$$H^+ + CO_3^{2-} \rightarrow CO_3^{-\bullet} \tag{17}$$

$$OH^- + HSO_5^- \rightarrow SO_5^{2-} + H_2O \tag{18}$$

$$SO_5^{2-} + HCO_3^- \rightarrow HCO_4^- + SO_4^{2-} \tag{19}$$

$$HSO_5^- + Cl^- \rightarrow SO_4^{2-} + HClO \tag{20}$$

$$HSO_5^- + 2Cl^- + H^+ \rightarrow SO_4^{2-} + Cl_2 + H_2O \tag{21}$$

$$Cl_2(aq) + H_2O \rightarrow HClO + H^+ + Cl^- \tag{22}$$

$$HClO \rightarrow ClO^- + H^+ \tag{23}$$

$$NO_3^- + OH^{\bullet} \rightarrow NO_3^{\bullet} + OH^- \tag{24}$$

$$NO_3^- + SO_4^{-\bullet} \rightarrow NO_3^{\bullet} + SO_4^{2-} \tag{25}$$
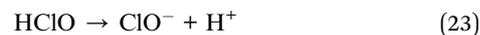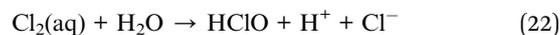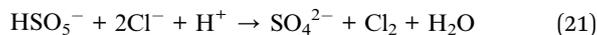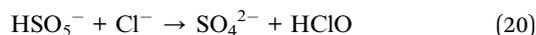
3.4 Identification and generation mechanism of active species

3.4.1 Identification of active species in systems. An active species quenching test was carried out to identify important free radicals and explore their reaction mechanism in the UV + nano-NiFe$_2$O$_4$/PMS system. First, 50 mM methanol (MeOH) was used to capture $SO_4^{-\bullet}$ and $OH^{\bullet}$,[57] 50 mM tert-Butanol (TBA) was used to quench $OH^{\bullet}$ (ref. 58) and 50 mM furfuryl alcohol was
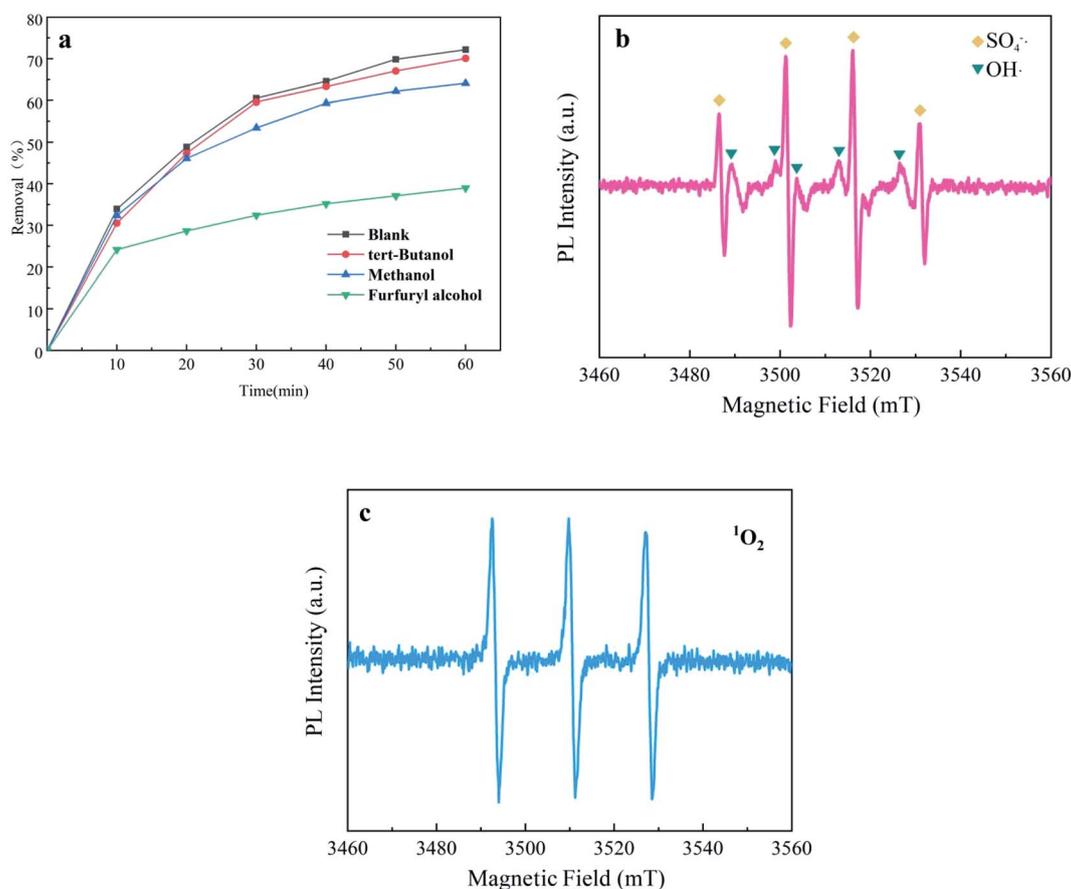
Fig. 5 Identification of radicals by different quenching agents (a); EPR spectra of $OH^{\bullet}$, $SO_4^{-\bullet}$ (b) and $^1O_2$ (c) formed after 60 min in the UV + nano-NiFe$_2$O$_4$/PMS system; the above experimental condition: [nano-NiFe$_2$O$_4$] = 1 g L^{-1}, [CTH] = 60 mg L^{-1}, [PMS] = 1 g L^{-1}, [UV wavelength] = 254 nm, pH = 2.7.

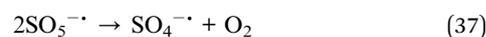employed to capture $^1O_2$. As presented in Fig. 5a, in the UV + nano-NiFe$_2$O$_4$/PMS systems with TBA and MeOH added, the removal efficiency of CTH was slightly reduced that respectively decreased from 72.0% to 70.01% and from 72.0% to 64.11%, proving that OH· and SO$_4^{-·}$ played a smaller role. However, compared with that in the system without any addition, the removal efficiency of CTH decreased from 72.0% to 38.9% after adding furfuryl alcohol into the system, indicating that $^1O_2$ greatly contributed to the CTH degradation process. To speculate on the mechanism of PMS activation by the UV + nano-NiFe$_2$O$_4$/PMS system, an EPR test was performed. EPR spectroscopy coupled with DMPO and TEMP as spin-trapping agents was applied to identify the free radicals generated in the system. The results of the EPR study are presented in Fig. 5b and c. It is obvious that characteristic signals are present in the EPR spectra of experiments conducted with DMPO and TEMP. DMPO–SO$_4$ and DMPO–OH signals were found after PMS activation by UV + nano-NiFe$_2$O$_4$ (Fig. 5b). More importantly, a strong ch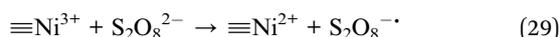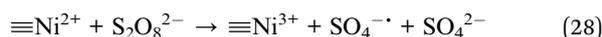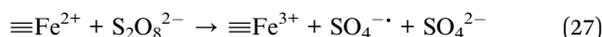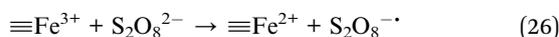aracteristic triplet signal of TEMP-$^1O_2$ was observed (Fig. 5c), which further confirmed the presence of $^1O_2$ in the UV + nano-NiFe$_2$O$_4$/PMS oxidation system. The EPR results were consistent with those of the active species quenching test.

3.4.2 Generation mechanism of active species. On the basis of the above analysis, a possible mechanism for free radical generation over the UV + nano-NiFe$_2$O$_4$/PMS system was proposed. The Ni^{2+} and Fe^{3+} ions on the surface of the catalyst could directly interact with S$_2$O$_8^{2-}$ to produce SO$_4^{-·}$ [eqn (26)–(29)]. Some of the dissolved Ni^{2+} could interact with water to produce the intermediate NiOH$^+$, which could promote the conversion of PMS to SO$_4^{-·}$ [eqn (30) and (31)]; SO$_4^{-·}$ reacted with H$_2$O to generate a large amount of OH· [eqn (32)]; OH· reacted with SO$_4^{-·}$ to produce HSO$_5^-$; and HSO$_5^-$ reacted with OH· and SO$_4^{-·}$ to form SO$_5^{-·}$. At the same time, the Ni^{3+} on the surface of the catalyst and in the aqueous solution could react with HSO$_5^-$ to form Ni^{2+} and SO$_5^{-·}$ [eqn (33)–(36)], and SO$_5^{-·}$ in the solution could also produce the same amount of SO$_4^{-·}$ [eqn (37)]. Then, a large amount of $^1O_2$ could be produced under the action of HSO$_5^-$ and SO$_5^{2-}$ and SO$_5^{-·}$ and water [eqn (38) and (39)]. Finally, under the action of SO$_4^{-·}$, OH· and $^1O_2$, CTH was degraded and mineralized into CO$_2$ and H$_2$O and thereby completely degraded [eqn (40)]. The proposed mechanism of PMS activation and CTH degradation is shown in eqn (26)–(40) as follows:

$$\equiv Fe^{3+} + S_2O_8^{2-} \rightarrow \equiv Fe^{2+} + S_2O_8^{-·} \tag{26}$$

$$\equiv Fe^{2+} + S_2O_8^{2-} \rightarrow \equiv Fe^{3+} + SO_4^{-·} + SO_4^{2-} \tag{27}$$

$$\equiv Ni^{2+} + S_2O_8^{2-} \rightarrow \equiv Ni^{3+} + SO_4^{-·} + SO_4^{2-} \tag{28}$$

$$\equiv Ni^{3+} + S_2O_8^{2-} \rightarrow \equiv Ni^{2+} + S_2O_8^{-·} \tag{29}$$

$$Ni^{2+} + H_2O \rightarrow NiOH^+ + H^+ \tag{30}$$

$$NiOH^+ + HSO_5^- \rightarrow NiOH^{2+} + SO_4^{-·} + OH^- \tag{31}$$

$$SO_4^{-·} + H_2O \rightarrow OH· + SO_4^{2-} + H^+ \tag{32}$$

$$OH· + SO_4^{-·} \rightarrow HSO_5^- \tag{33}$$

$$HSO_5^- + SO_4^{-·} \rightarrow SO_5^{-·} + SO_4^{2-} + H^+ \tag{34}$$

$$HSO_5^- + OH· \rightarrow SO_5^{-·} + H_2O \tag{35}$$

$$\equiv Ni^{3+} + HSO_5^- \rightarrow \equiv Ni^{2+} + SO_5^{-·} + H^+ \tag{36}$$

$$2SO_5^{-·} \rightarrow SO_4^{-·} + O_2 \tag{37}$$

$$HSO_5^- + SO_5^{2-} \rightarrow SO_4^{2-} + HSO_4^- + {}^1O_2 \tag{38}$$

$$2SO_5^{-·} + H_2O \rightarrow 2HSO_4^- + 1.5{}^1O_2 \tag{39}$$

$$SO_4^{-·} + OH· + {}^1O_2 + CTH \rightarrow CO_2 + H_2O \tag{40}$$
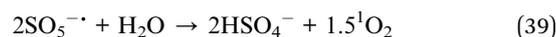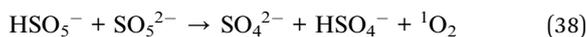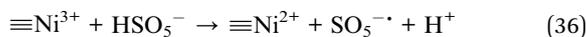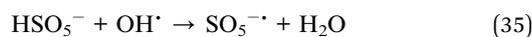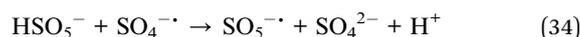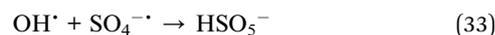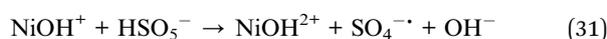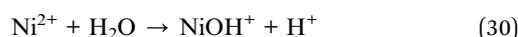
3.5 Degradation mechanism of CTH in the UV + nano-NiFe$_2$O$_4$/PMS system

3.5.1 UV-vis spectral analysis in the degradation process of CTH. The UV-vis spectrum of the degradation process of CTH is shown in Fig. 6. CTH contains a conjugate composed of a benzene ring, ketone group and enol system, and its structure has 2 chromophores. At the beginning of the reaction, there were 3 obvious absorption bands at approximately 229 nm, 269 nm and 366 nm. These bands corresponded to 4 different ring structures in the molecular structure. After the reaction started, the intensities of these characteristic peaks continued to decrease. This decrease showed that the degradation of CTH was a gradual oxidative degradation process. In particular, the absorption peak at 366 nm showed a certain degree of blueshift after 30 min of reaction. This blueshift indicated that the benzene ring structure of CTH was progressively destroyed. This damage first occurred at the unsaturated bond position of the benzene ring, and then, the benzene ring generated a series of small-molecule intermediate products through ring opening and oxidation.[31]

3.5.2 Degradation products and degradation pathway. The possible intermediate products formed during the CTH degradation process in the UV + nano-NiFe$_2$O$_4$/PMS system were determined by LC-MS. As shown in Fig. 7, nine reactive
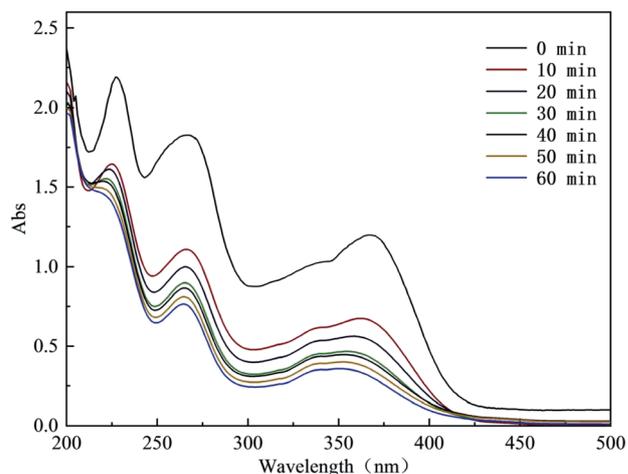

Fig. 6 UV-visible spectrum in the degradation process of CTH.

intermediates were possibly observed, and the structures are listed; the transformation pathway was proposed accordingly. In transformation pathway 1, first, the two methyl groups on the N atom were removed to form product A ($m/z = 450$), and then, C4 underwent deamination to produce product D ($m/z = 435$), after which C2 underwent deamination to produce product E ($m/z = 392$) and was finally oxidized to open the ring to produce product F ($m/z = 370$). The methyl group in the dimethylamino moiety was eliminated, which might be due to direct UV photolysis[59] or OH[·] and $SO_4^{-·}$ induced hydrogen atom extraction from the methyl substituent.[60] The hydroxylation of

transformation pathway 2 is a common reaction route in the $SO_4^{-·}$ reaction mechanism that produces product B ($m/z = 494$). $SO_4^{-·}$ has a similar reaction mechanism to HO[·], namely, (i) hydrogen abstraction; (ii) addition of hydroxyl groups to unsaturated carbons including double bonds and aromatic rings; and (iii) electron transfer.[61,62] The unsaturated double bond of CTH was attacked to form a hydroxylate species. The C6 and C8 sites were prone to undergo dehydration reactions;[60] hence, dehydration occurred and produced product C ($m/z = 460$) in transformation pathway 3. Eventually, CTH was degraded into structurally simple products [product G ($m/z =$
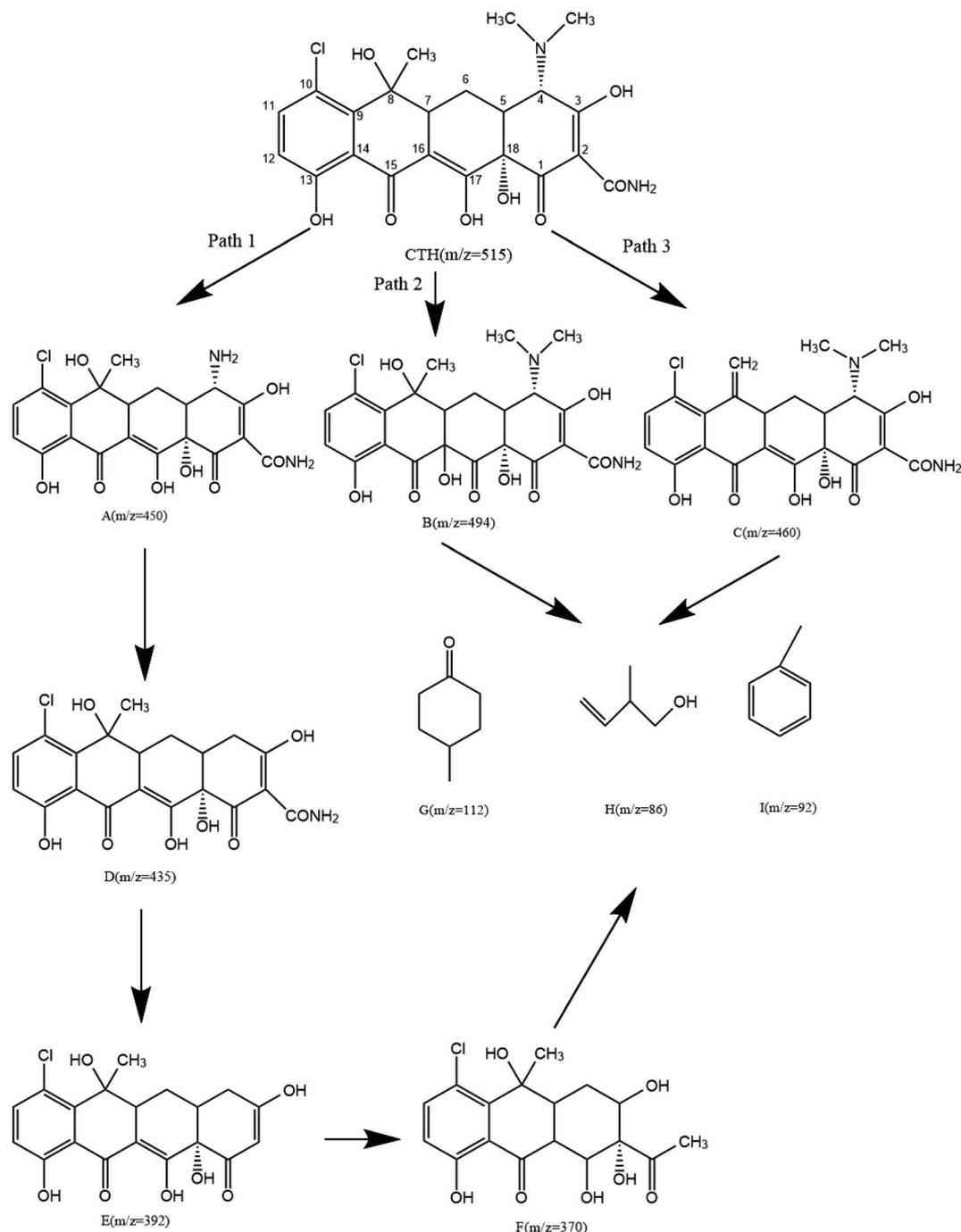

Fig. 7   The degradation pathway of CTH in the UV + nano-NiFe$_2$O$_4$/PMS system.

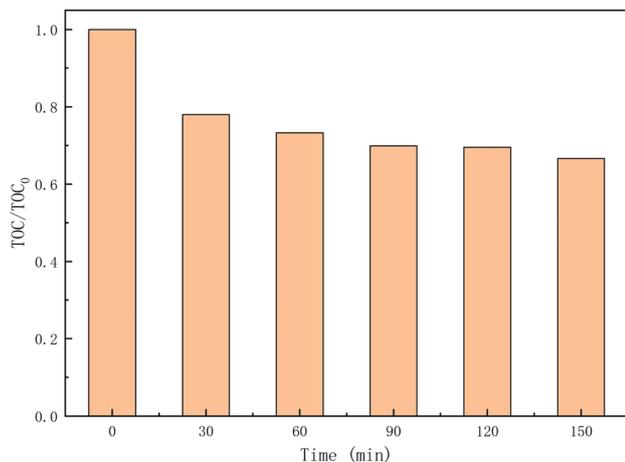**Fig. 8** TOC removal in the UV + nano-NiFe$_2$O$_4$/PMS system; the experimental condition: [nano-NiFe$_2$O$_4$] = 1 g L^{-1}, [CTH] = 60 mg L^{-1}, [PMS] = 1 g L^{-1}, [UV wavelength] = 254 nm, pH = 2.7.

112), product H (m/z = 86), and product I (m/z = 92)] and was ultimately mineralized into CO$_2$ and H$_2$O.

3.5.3 TOC removal in the degradation process of CTH. As an indicator of water quality, the mineralization test is an important assessment to obtain information on the degradation of the TOC.[63] To explore the mineralization of CTH in the UV + nano-NiFe$_2$O$_4$/PMS system, the TOC was monitored from 0 to 150 min, and the results are shown in Fig. 8. As the reaction progressed, the TOC in the system showed a slow downward trend, decreasing by 22% after 30 min, and then, the TOC ultimately tended to stabilize, which may be caused by insufficient oxidant in the system. With time, the mineralization rate of TOC reached 33%, indicating that the UV + nano-NiFe$_2$O$_4$/PMS system could degrade CTH to generate CO$_2$ to some extent under the conditions employed for testing the performance of this process. While the TOC decreased and reached stability, CTH experienced three possible degradation pathways, namely, (i) demethylation and deamination; (ii) hydroxylation; and (iii) dehydration. Finally, CTH was oxidized to open the ring to produce simple products, some of which were mineralized into CO$_2$ and H$_2$O. However, only part of the CTH was completely mineralized, and the rest have been converted into other products that were more difficult to degrade than CTH.

4. Conclusions

In summary, we successfully synthesized nano-NiFe$_2$O$_4$ by *via* a hydrothermal synthesis method and demonstrated that nano-NiFe$_2$O$_4$ as a catalyst combined with UV irradiation activation PMS can effectively degrade CTH. The following were our main conclusions:

(1) The SEM, XRD and FTIR results confirmed that nano-NiFe$_2$O$_4$ consisted of loose nano-microstructure particles and exhibited high stability.

(2) The heterogeneous system of UV + nano-NiFe$_2$O$_4$/PMS had a better effect on the removal of CTH than other parallel systems. By exploring the factors affecting the reaction process, it was found that the optimum dosages of nano-NiFe$_2$O$_4$ (1 g L^{-1}), PMS

(1 g L^{-1}), CTH (60 mg L^{-1}) and pH (11) at UV wavelength of 254 nm afforded a high removal efficiency of approximately 96%. The five anions coexisting in the solution, Cl$^-$, HCO$_3^-$, CO$_3^{2-}$ and NO$_3^-$, could increase CTH degradation by 21.29%, 27.17%, 25.32% and 5.96% respectively, while H$_2$PO$_4^-$ could inhibit CTH degradation and the removal efficiency decreased 6.08%.

(3) The active species quenching tests and EPR analysis proved that ^{1}O$_2$ contributed greatly to the CTH removal process and that OH$^\cdot$ and SO$_4^{-\cdot}$ had a small impact on the CTH removal efficiency.

(4) Nine different byproducts were identified *via* LC-MS. The degradation of CTH was mainly caused by hydroxylation, demethylation, deamination and dehydration. This study showed that only 33% of TOC was mineralized, proving that only part of the CTH was completely mineralized and that the rest might have been converted into other products that were more difficult to degrade than CTH.

This work systematically investigated the effect of different reaction parameters on the degradation of CTH and provided a comprehensive description of the degradation of CTH in the UV + nano-NiFe$_2$O$_4$/PMS system. Therefore, our results provide a theoretical basis for the development of large-scale degradation of CTH. Nevertheless, to apply these processes, not only should the degradation efficiency be considered but also the overall investment, operation, and maintenance costs.

Conflicts of interest

There are no conflicts to declare.

Acknowledgements

References

1 V. K. Gupta, I. Ali, T. A. Saleh, A. Nayaka and S. Agarwalc, *RSC Adv.*, 2012, **2**, 6380–6388.

2 A. A. Ahmed, T. A. Saleh, A. M. Ajeebi, M. S. A. Gharsan and N. F. Aldahmash, *Biotechnol. Prog.*, 2019, **36**, e2907.

3 A. A. Alswat, M. B. Ahmad and T. A. Saleh, *Colloid Interface Sci.*, 2017, **16**, 19–24.

4 V. K. Gupta, D. Pathania, M. Asif and G. Sharma, *J. Mol. Liq.*, 2014, **196**, 107–112.

5 Y. J. Tian, J. R. Zou, F. Li, L. Q. Zhang and Y. Z. Liu, *Water Res.*, 2019, **149**, 35–41.

6 H. Wang, Y. Wu, M. B. Feng, W. G. Tu and T. Xiao, *Water Res.*, 2018, **144**, 215–225.

7 R. Pulicharla, R. K. Das, S. K. Brar, P. Drogui and R. Y. Surampalli, *Chem. Eng. J.*, 2018, **347**, 828–835.

8 B. Liu, Y. X. Li, X. L. Zhang, J. Wang and M. Gao, *Eur. J. Soil Biol.*, 2015, **68**, 69–76.

9 R. X. Guo and J. Q. Chen, *Chemosphere*, 2012, **87**, 1254–1259.

10 S. C. Anderson, S. Subbiah, A. Gentles, D. Oliver, P. Stonum, T. A. Brooks and E. E. Smith, *J. Chromatogr. B: Anal. Technol. Biomed. Life Sci.*, 2018, **1092**, 237–243.

11 X. H. Peng, J. R. Cao, B. L. Xie, M. S. Duan and J. C. Zhao, *Ecotoxicol. Environ. Saf.*, 2020, **188**, 109869.

12 J. L. Zhang and Z. Ma, *J. Chem. Eng.*, 2018, **26**, 753–760.

13 Y. Sun, X. J. Wang, S. Q. Xia and J. F. Zhao, *Chem. Eng. J.*, 2021, **416**, 129085.

14 Y. T. Lin, C. Liang and C. W. Yu, *Ind. Eng. Chem. Res.*, 2016, **55**, 2302–2308.

15 T. A. Saleha, S. Agarwal and V. K. Guptaa, *Appl. Catal., B*, 2011, **106**, 46–53.

16 S. Karthikeyan, V. K. Gupta, R. Boopathy, A. Titus and G. Sekaran, *J. Mol. Liq.*, 2012, **173**, 153–163.

17 M. Qamar, M. O. Fawakhiry, A. M. Azad, M. I. Ahmed, A. Khana and T. A. Saleh, *RSC Adv.*, 2016, **6**, 71108–71116.

18 Y. H. Lee and V. G. Urs, *Water Res.*, 2010, **44**, 555–566.

19 C. j. Liang, C. J. Bruell, M. C. Marley and K. L. Sperry, *Chemosphere*, 2004, **55**, 1213–1223.

20 B. Muhammad, A. Muhammad, R. Tahir and Y. Q. Zha, *Environ. Int.*, 2019, **124**, 336–353.

21 S. Y. Oh, H. W. Kim, J. M. Park, H. S. Park and C. Yoon, *J. Hazard. Mater.*, 2009, **168**, 346–351.

22 J. M. Monteagudo, A. Durán, R. González and A. J. Expósito, *Appl. Catal., B*, 2015, **176**, 120–129.

23 B. Rishikesh and S. W. Jeong, *Chemosphere*, 2021, **270**, 128627.

24 M. J. Xu, H. Y. Zhou, Z. L. Wu, N. W. Li, Z. K. Xiong, G. Yao and B. Lai, *J. Hazard. Mater.*, 2020, **399**, 123103.

25 A. O. Salawudeen, B. S. Tawabini, A. M. Al-Shaibani and T. A. Saleh, *Environ. Nanotechnol. Monit. Manage.*, 2020, **13**, 100288.

26 T. A. Saleh, *Appl. Surf. Sci.*, 2011, **257**, 7746–7751.

27 T. A. Saleh, *J. Cleaner Prod.*, 2018, **172**, 2123–2132.

28 T. Prabhakaran and J. Hemalatha, *Ceram. Int.*, 2014, **40**, 3315–3324.

29 G. Fadillah, W. P. Wicaksono and T. A. Saleh, *Microchem. J.*, 2020, **159**, 105353.

30 Y. M. Lee, G. Lee and K. Duk, *J. Hazard. Mater.*, 2021, **403**, 123591.

31 H. X. Huang, T. Guo, K. Wang, Y. Li and G. K. Zhang, *Sci. Total Environ.*, 2021, **758**, 143957.

32 J. He, J. C. Tang, Z. Zhang, L. Wang, Q. L. Liu and X. M. Liu, *Chem. Eng. J.*, 2021, **404**, 126997.

33 B. Y. Yan, D. C. Xu, Z. Q. Liu, J. Z. Tang, R. Huang, M. Zhang, F. Y. Cui, W. X. Shi and C. Hu, *Chem. Eng. J.*, 2021, **404**, 127041.

34 V. C. Mora, J. A. Rosso, G. C. L. Roux, D. O. Mártire and M. C. Gonzalez, *Chemosphere*, 2009, **75**, 1405–1409.

35 A. T. Pereira, P. C. Henriques, P. C. Costa, M. C. L. Martins, F. D. Magalhães and I. C. Gonçalves, *Compos. Sci. Technol.*, 2019, **184**, 107819.

36 P. He, J. Y. Zhu, Y. Z. Chen, F. Chen, Z. L. Zhu, M. F. Liu, K. Zhang and M. Gan, *Chem. Eng. J.*, 2021, **406**, 126758.

37 C. K. O. d. Silva-Rackov, W. A. Lawal, P. A. Nfodzo, M. M. G. R. Vianna, C. A. O. d. Nascimento and H. Choi, *Appl. Catal., B*, 2016, **192**, 253–259.

38 C. Q. Gao, W. Yu, Y. C. Zhu, M. Wang, Z. Z. Tang, L. Du, M. Y. Hu, L. Fang and X. C. Xiao, *Sci. Total Environ.*, 2021, **754**, 142131.

39 A. Ghauch, A. Baalbaki, M. Amasha, R. E. Asmar and O. Tantawi, *Chem. Eng. J.*, 2017, **317**, 1012–1025.

40 C. S. D. Rodrigues and L. M. Madeira, *Environ. Technol. Innovation*, 2021, **21**, 101265.

41 X. Gu, S. Lu, L. Li, Z. Qiu, Q. Sui, K. Lin and Q. Luo, *Ind. Eng. Chem. Res.*, 2011, **50**, 11029–11036.

42 H. P. Gao, J. B. Chen, Y. L. Zhang and X. F. Zhou, *Chem. Eng. J.*, 2016, **306**, 522–530.

43 Z. Wang, G. H. Chen, X. R. Wang, G. H. Yang, Y. Liu and C. Zhang, *J. Hazard. Mater.*, 2021, **401**, 123378.

44 C. M. Dominguez, V. Rodriguez, E. Montero, A. Romero and A. Santos, *Sep. Purif. Technol.*, 2020, **241**, 116679.

45 P. Xiao, L. An and D. Wu, *New Carbon Mater.*, 2020, **35**, 667–683.

46 G. V. Buxton, C. L. Greenstock, W. P. Helman and A. B. Ross, *J. Phys. Chem. Ref. Data*, 1988, **17**, 513–886.

47 A. Ahmad, X. G. Gu, L. Li, S. G. Lv, Y. S. Xu and X. H. Guo, *Environ. Sci. Pollut. Res.*, 2015, **22**, 17876–17885.

48 J. Q. Wang, Q. R. Qian, Q. H. Chen, X. P. Liu, Y. J. Luo, H. Xue and Z. H. Li, *Chin. J. Catal.*, 2020, **41**, 1511–1521.

49 M. H. Nie, Y. Yang, Z. J. Zhang, C. X. Yan, X. N. Wang, H. J. Li and W. B. Dong, *Chem. Eng. J.*, 2014, **246**, 373–382.

50 G. D. Fang, D. D. Dionysiou, D. M. Zhou, Y. Wang, X. D. Zhu, J. X. Fan, L. Cang and Y. J. Wang, *Chemosphere*, 2013, **90**, 1573–1580.

51 F. Aqsa, S. Karunamoorthy, K. Talukdar, Y. Kim, Y. Yoon and C. M. Park, *Chem. Eng. J.*, 2021, **407**, 127842.

52 T. Zhang, H. B. Zhu and C. J. Philippe, *Environ. Sci. Technol.*, 2013, **47**, 2784–2791.

53 H. Chen and K. C. Carroll, *Environ. Pollut.*, 2016, **215**, 96–102.

54 P. Neta, V. Madhavan, H. Zemel and R. W. Fessenden, *J. Am. Chem. Soc.*, 1977, **99**, 163–164.

55 S. Padmaja, Z. Alfassi, P. Neta and R. Huie, *Int. J. Chem. Kinet.*, 1993, **25**, 193–198.

56 M. H. Nie, C. X. Yan, M. Li, X. N. Wang, W. L. Bi and W. B. Dong, *Chem. Eng. J.*, 2015, **279**, 507–515.

57 P. Neta, J. Grodkowski and A. B. Ross, *ChemInform*, 1996, **27**, 1027–1284.

58 G. P. Anipsitakis and D. D. Dionysiou, *Environ. Sci. Technol.*, 2004, **38**, 3705–3712.

59 F. Yuan, C. Hu, X. X. Hu, D. B. Wei, Y. Chen and J. H. Qu, *J. Hazard. Mater.*, 2011, **185**, 1256–1263.

60 J. P. Wang, M. Zhang, R. J. Zhou, J. Y. Li, W. Zhao and W. Y. Chen, *J. Environ. Chem. Eng.*, 2021, **9**, 104907.

61 T. C. Liu, K. Yin, C. B. Liu, J. M. Luo, C. John, W. Q. Zhang, S. L. Luo, Q. Y. He, Y. X. Deng, H. Liu and D. Y. Zhang, *Water Res.*, 2018, **147**, 204–213.

62 Y. Q. Liu, X. X. He, Y. S. Fu and D. D. Dionysiou, *J. Hazard. Mater.*, 2016, **305**, 229–239.

63 C. Y. Shao, R. B. Zhao, S. Q. Jiang, S. S. Yao, Z. F. Wu, B. Jin, Y. L. Yang, H. H. Pan and R. K. Tang, *Adv. Mater.*, 2018, **30**, 1704867.